THE ANNALS OF "DUNAREA DE JOS" UNIVERSITY OF GALATI.
FASCICLE IX. METALLURGY AND MATERIALS SCIENCE
N^0. 4 – 2012, ISSN 1453 – 083X

SYNTHESIS AND CHARACTERISATION OF Ag/SnO_2/CLAY NANOCOMPOSITES WITH POTENTIAL APPLICATION AS PHOTOCATALYSTS

Claudia-Mihaela HRISTODOR, Diana TANASA, Narcisa VRINCEANU, Violeta-Elena COPCIA, Aurel PUI, Eveline POPOVICI
"Al.I.Cuza" University of Iasi
email: narcisa.vrinceanu@ulbsibiu.ro

ABSTRACT

This work reported a novel synthesis and characterization of Ag/SnO_2/clay nanocomposites. The obtained materials were characterized using techniques such as X-ray diffraction (XRD), Fourier Transform Infrared Spectroscopy, particles size distribution, BET analyses and Scanning Electron Microscopy. The Ag/SnO_2/clay nanocomposites have been used as efficient and environmentally benign photocatalysts. The protocols developed using this kind of material is advantageous in terms of simple experimentation, reusable catalyst, excellent yields of the products, short reaction time and preclusion of toxic solvents. The synthesized nanosized AgSnO_2/clay nanocomposites have been used as photocatalysts for degradation and discoloration of synthetic wastewater containing Eosin Y dye, xanthene fluorescent dye, under solar radiation.

KEYWORDS: clay, nanocomposite, dye, wastewater

1. Introduction

A great variety of methods have been used in recent years to synthesize nano powders of oxide materials and especially semiconducting powders like TiO2, MgO, Fe_2O_3, SnO_2 and ZnO. Nano-sized tin oxide (SnO_2) is an interesting semiconducting material with a wide band gap (Eg = 3.6 eV, at 25^{o}C) [1]. Nanoparticles of tin oxide have found a wide range of applications in gas sensors, lithium batteries, optoelectronic devices, transparent electrodes and photocatalysts [2-8]. It is generally known that by changing the method of preparation it is possible to change the structural, morphological and textural properties of metal oxide particles.

A very promising candidate for such an application is represented by the system silver tin oxide [9]. The noble metals deposited on the surface of nano oxide powders can improve its photo-catalytic properties.

There has been very limited study in this direction. The researches on the preparation of silver nanoparticles have been an extraordinarily active area due to its potential applications in nanoelectronics, magnetics, biosensor, data storage, catalysis, surface enhanced Raman scattering and excellent antibacterial activity [10–15]. Most of these applications require nanoparticles with a small particle size and a narrow size distribution [16, 17].

To the best of our knowledge, there has been no publication on the synthesis of the Ag/SnO_2/clay nanocomposites. The present method for silver nanoparticles preparation is not only the formation rate of silver nanoparticles much quicker, particle size distribution more uniform, but also offers numerous benefits of eco-friendliness and compatibility for pharmaceutical and biomedical applications due to all the environmentally benign and renewable materials used in the experiments are [18].

Metals or semiconductor nanoparticles synthesized by various techniques have found potential application in many fields such as catalysis, sensors, etc. [19 -22]. In most of the applications, nanoparticles are used as building blocks toward functional nanostructures. The coinage metal nanoparticles such as silver, gold, and copper are mostly exploited for such purposes as they have surface plasmon resonance absorption in the UV visible region [23]. The surface plasmon band arises from the coherent existence of free electrons in the conduction band due to the small particles size effect, which is dependent on the particle sizes, chemical surrounding, adsorbed species on the surface, and dielectric constant [23-26]. The unique feature of the

coinage metal nanoparticles is that a change in the absorbance or wavelength provides a measure of the particle size, shape, and interparticle properties. For small particles (2 nm), the surface plasmon band is strongly damped due to low electron density in the conduction band. However, as particle size increases, the intensity of the surface plasmon band increases. It has been suggested that, although both absorbance and scattering contribute to the optical property, the contribution of the latter is relatively insignificant as compared to that of the former for very small nanoparticles (e15 nm). [19-33]

2. Experimental Methods

2.1. The starting material

As raw material, we used clay of montmorillonite bentonite type, provided by firma Riedel-de Haen Chemicals Company. Given the compositional complexity of clay materials, we considered useful to perform an ion exchange process, as a first step, for their cleansing, their transition to sodium cation form, respectively. The clay exchange in Na^+ form has been performed by treating it with a 1M NaCl solution, having a solid/liquid ratio of 1:10 [34, 35].

2.2. Preparation of Ag/SnO_2/clay nanocomposites

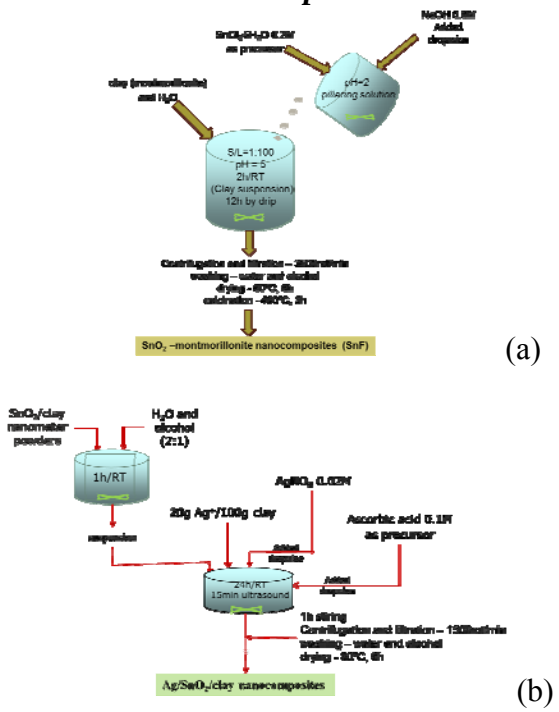

Fig. 1. *Schematic illustration for preparation of nanosized Ag/SnO_2/clay compounds (AgSnF)*

Bentonite montmorillonitic-clay, provided by Riedel-de Haen Chemicals Company, was used as starting material. The nanosized SnO_2 particles were prepared by pillaring method (dispersing the tin oxide particles). Preparation of Ag/SnO_2/clay nanocomposites takes place in two steps preparation of SnO_2/clay nanometer powders (Fig. 1, a) and obtaining of Ag/SnO_2/clay nanocomposites shown in Fig. 1, b.

2.3. Studies of photocatalysis

Investigations of photocatalytic oxidation have been performed, having as objective degradation and discoloration of synthetic solution containing Eosin Y dye, by varying the concentration of catalyst (0,5-2g/l). Photocatalysis occurs in two stages: the first step consists in adsorption in the dark conditions, for 30 minutes and the second step relies on photometric measurement of the dye concentration, by exposure to UV light running at wavelength of 254 nm at equal time intervals based on the calibration curve.

The study was conducted in an initial concentration of pollutant (Eosin Y dye) in water of 20 mg/L, using nanometer SnO_2 as photocatalyst. Other working conditions are as follows: for photocatalysis 1g catalyst/L, 2g catalyst/L respectively, have been used, at an initial pH=5.5±0,2, temperature 25°C±2°C. Photocatalytic test was done using a type of UV lamp UVP, 254 nm surface. Photocatalyst sample was stirred for 30 min to reach equilibrium and then coupled to the UV lamp and the timer was turned on.

2.4. Characterization methods

The structure and properties of the obtained materials were studied by X Ray Diffraction (XRD), FTIR spectroscopy, N_2 adsorption-desorption isotherms and UV–Vis diffuse reflectance spectroscopy. The structures of pure and modified clay were investigated using Shimadzu LabX XRD 6000 diffractometer. The diffraction angle was scanned from 10 to 80 degrees, an usual interval for complex clays and SnO_2. Measurement conditions were: X-ray tube, Cu target Cu, voltage = 40.0 (kV), current 30.0 (mA) and scanning: scan mode-Continuous Scan, scan speed 2.0000 (deg/min). FTIR spectra were recorded on a FTIR JASCO 660+ spectrometer. UV–vis diffuse reflectance spectra recording was performed by a Shimadzu UV-2401 PC Recording Spectrophotometer ranging between 200–600 nm. The adsorption isotherms of N_2 , specific surface areas and porosities were determined with a Nova 2200e (Quantachrome Instruments) automated sorptometer at 77 K. Particles size distribution and mean particle size diameter (D_p, nm) measurements were recorded using an optic

measurement device SALD-7001 type Laser Diffraction Particle Size Analyzer (Shimadzu, Japan).

3. Results and Discussion

Changes occurring in the structure of lamellar supports can be monitored on the basis of Bragg reflections determined from the X-ray diffractograms of the Ag/SnO_2/layer silicate samples.

Identification of peaks was performed using the diffractometer software. The pure clay presents all specific peaks for complex clays: quartz, bentonite, feldspar, aluminum silicate and mica. Reference diffractogram for thin oxide shows a nanocrystalline powder with tetragonal structure of elementary cell. These elementary cell dimensions are well fitted in SiO_2 sites of clay, as identification image shows. Thus, the stable monodisperse, uniform particle size distribution of silver nanoparticles ise formed.

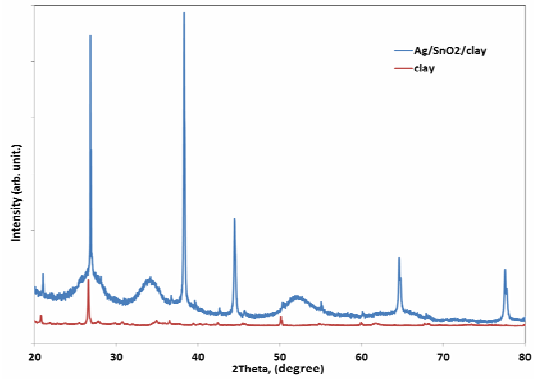

Fig. 2. *X-ray diffraction (XRD) patterns of the studied samples*

X-ray diffraction patterns of clay and Ag/SnO_2/clay nanocomposites have been given in Fig. 2. The crystallite sizes of these samples were obtained by using Scherrer's equation. D = kk/bcosh where D is the crystallite size, k is the radiation wavelength (1.5406 Å), b is the peak full width at half maximum (FWHM), h is the diffracting angle and k = 0.94 for spherical shape particle. The average crystallite size was found to be 18.17Å and 11.75Å (±1) nm, respectively for clay and Ag/SnO_2/clay nanocomposites mode powder. As shown in Fig. 2 the original d-spacing of clay, 3.32Å and 2.34Å of Ag/SnO_2/clay nanocomposites 2θ angles (2θ = 26.82° and 38.29Å respectivelly).

This value is a direct proof of the fact that, in the path of Ag^+ ions are bound not only on the external surfaces and edges of MMT but also in the interlamellar space. Since the ionic radius of Ag^+, is 1.22 Å it is expected that silver occupies interstitial position which in turn can lead to expansion of lattice parameters. We presume that some of the Ag^+ rests go to the surface of the clay.

The IR spectra of the clay and Ag/SnO_2/clay nanocomposites are shown in Figure 3. The band situated at 3614 cm^{-1} is specific to montmorrilonite by its elongation vibrations belonging to OH groups from octahedral layer coordinated, the 1014 cm^{-1} and 1025 cm^{-1} wavelength specific to Si-OH sylanolic groups from the material surface and the 784 cm^{-1} wavelength specific to the deformation vibration of O-H group, bound by an Al-Al-OH cation.

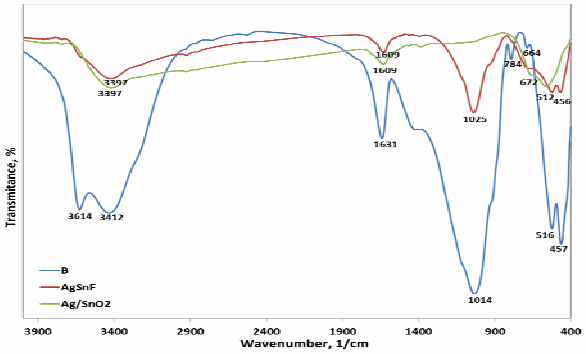

Fig. 3. *FTIR Spectra: B – clay; AgSnF – Ag/SnO_2/clay nanocomposites; Ag/SnO_2 – Ag/SnO_2 nanoparticles*

At the O–H stretching frequency region, all the impregnation and pillared clay materials show two intense IR 3412 cm^{-1} (Fig. 3). These two bands have been assigned to the stretching vibration of the structural OH groups in the clay sheet and to the water molecules present in the interlayer, respectively [36, 37]. If one compares the intensity of these bands for the clay samples, note that the pillaring has a positive impact on the water retention capacity of the clay minerals and the intensity of the band descreases with the process of pillaring. [38]

The IR band observed at 1631 cm^{-1} is due to the bending vibration mode of OH groups. Montmorillonite clay is known to contain two types of hydroxyl groups. One of them is more labile, with an IR absorption pattern similar to that of liquid water and has been ascribed to the water molecules present in the outer coordination spheres of the interlayer cations. The other type is more firmly held and is associated with the water molecules directly coordinated to the exchangeable cations. The latter directly coordinated to the exchangeable cations. The latter is type also contributes significantly to this absorption band [36]. The hydrated aluminum species present in the clay interlayer contain significantly larger amounts of water molecules in the first coordination sphere. The intense band observed for the impregnation and pillared clay suggests the possibility of increasing the acidity due to pillaring since the water molecules in the first coordination sphere dissociate in the clay interlayer, producing

protons. The structural OH-bending mode in montmorillonite shows a series of discrete IR absorption bands between 784 cm^{-1} depending upon the cation composition in the octahedral sheet [39]. Fig. 4 shows bands around 3397 cm^{-1} and 1609 cm^{-1} for Ag/SnO_2 nanoparticles and Ag/SnO_2/clay nanocomposites.

Micromorphology and textural characteristics of clay and Ag/SnO_2/clay nanocomposites are described by the results of nitrogen adsorption/desorption isotherms. The specific surface area has been calculated using BET method at a relative pressure ranging between 0.05-0. The pore volume has been calculated at a relative pressure of 0.95. The distribution of pore size has been determined from the nitrogen adsorption isotherm using Barett-Joyner-Halenda model (BJH model). Subsequently, isotherms and distributions corresponding to the pore sizes have been performed (Fig. 4).

The general aspect of the samples isotherm reveals an IUPAC IV type isotherm, characteristic to the porous absorbers, presenting the so-called capilar condensation phenomenon. The results of pore distribution calculus (Fig. 4) indicate the occurrence of some mesoporous with 4.18nm and 3.73nm radius, respectively.

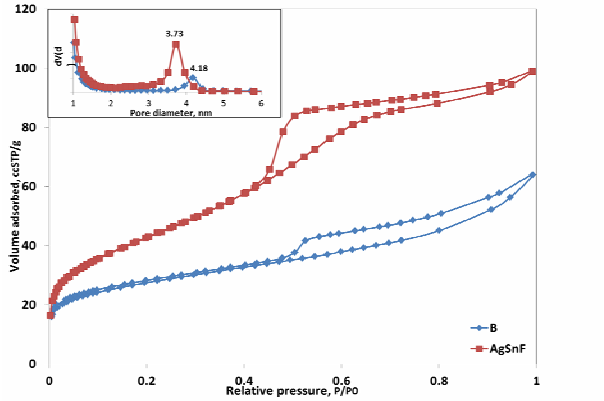

Fig. 4. *The N_2 adsorption/desorption isotherms of the clay (B) and Ag/SnO_2/clay nanocomposites (AgSnF)*

In the domain of partial pressures values higher than p/p_0>0,5 the isotherm unveils the appereance of an H3 type hysteresis, indicating the existence of pores with a relatively even distribution [40]. The amounts of adsorbed nitrogen measured at identical relative pressures are considerably higher in Ag/SnO_2/clay nanocomposites than in the bare clay support. In the Ag/SnO_2/clay nanocomposites samples, N_2 molecules have access to a much larger surface (the nanoparticles own surface also contributes to the overall increase in surface area) than it is the case in the unmodified support. [41]

Table 1. *Textural properties of the materials*

Sample	Surface area, $a_{s\ BET}$	Pore volume	Pore diameter
	[m^2/g]	[cc/g]	[nm]
B	97.206	0.127	4.18
AgSnF	153.471	0.267	3.73

From data in Table 1 data, it is noteworthy that after the intercalation of silver/tin oxide between the clay's interlayers the BET specific surface area, pore size and total volume increase, which confirm the fact that silver/tin oxide has been intercalated between the clay's interlayers.

The particle size distribution for clay and Ag/SnO_2/clay nanocomposites is shown in Fig. 5 and Fig. 6. For a sample two consecutive measurements were made. The particle size distribution of clay appeared to be bimodal, with particles averaging about 0.1 μm.

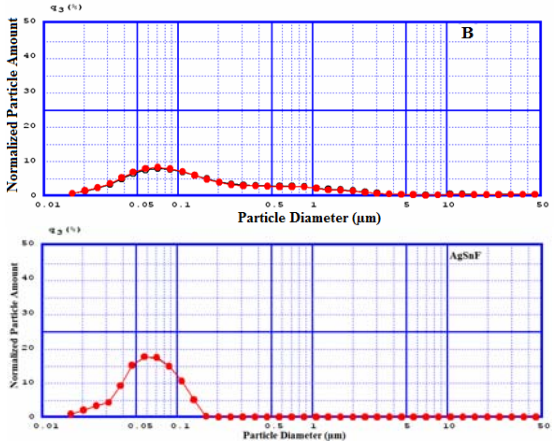

Fig. 5. *Volume histogram of the particle size distribution in clay (B) and Ag/SnO_2/clay nanocomposites (AgSnF)*

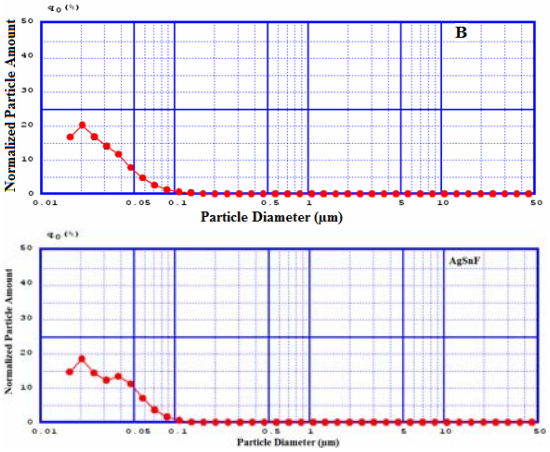

Fig. 6. *Numerical histogram of the particle size distribution in clay (B) and Ag/SnO_2/clay nanocomposites (AgSnF)*

Representing the numerical histogram we could say that the particle size distribution is unimodal with the particle diameter of 0.06μm.

We firstly checked the photocatalytic performance of the Ag/SnO_2/clay nanocomposites for degradation of Eosin Y dye. The results are shown in Fig. 7. Samples investigations of photocatalytic oxidation had as objective the degradation and discoloration of synthetic solution containing Eosin Y dye, by varying the concentration of catalyst: 1g/L and 2g/L respectively. Some blank experiments (without UV irradiation or catalysts) were carried out in order to check if the Eosin Y dye removal is really due to a photocatalytic process. The experiments conducted in the absence of photocatalyst but with the assistance of UV irradiation showed the fact that the Eosin Y cannot be degraded. The absorption spectra of the obtained Ag/SnO_2/clay nanocomposites are shown in Fig. 7. Eosin Y shows a mean absorption peak in visible region at 516 nm and the rate of decolorization was recorded with respect to the change in intensity of this absorption peak. The main absorption peak has diminished and finally disappeared during photoirradiation process, which indicated that the Eosin Y had been degraded.

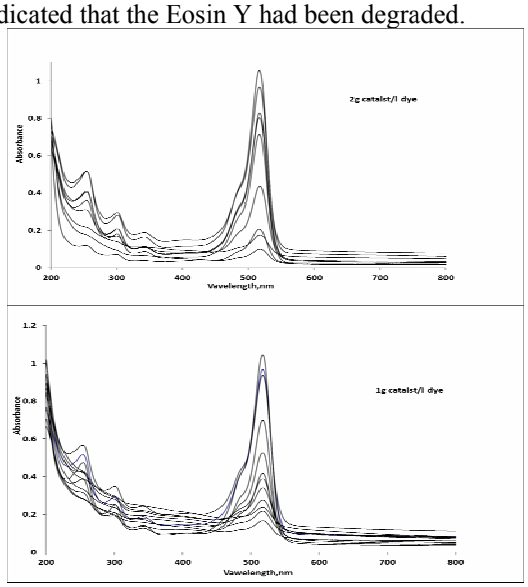

Fig. 7. *UV-vis spectra of the studied samples: 1-2g Ag/SnO_2/clay nanocomposites/L Eosin Y dye*

It is known that the photocatalysed decolourization of a dye in solution is initiated by the photoexcitation of the SnO_2, followed by the formation of electron–hole pair on the surface of catalyst. The high oxidative potential of the hole in the catalyst permits the direct oxidation of the dye to reactive intermediates.

Another reactive intermediate which is responsible for the degradation is hydroxyl radical (OH•). It is either formed by the decomposition of water or by reaction of the hole with OH^-. The hydroxyl radical is an extremely strong, non-selective oxidant (E_0 = +3.06V) which leads to the partial or complete mineralization of several organic chemicals [42, 43]. It can be seen that the loading of silver can significantly enhance the photocatalytic efficiency of SnO_2 in degradation of Eosin Y. The positive effect of noble metal deposits is commonly due to the fact that Ag nanoparticles on the semiconductor surface behave like electron sinks, which provides sites for accumulation of the photogenerated electrons, and then improves the separation of electrons and holes. This can be understood based on the proposed charge separation of Ag/ SnO_2under UV illumination. [44, 45]

An efficient photocatalytic process needs very crystalline semiconductors, in order to reduce the recombination electrons/positive holes pairs. Thus, for an increasing of catalyst quantity up to an optimal dose, a higher quantity leads to an augmentation of the efficiency of Eosin Y removal, due to the generation of a higher number of active species. The bigger the quantity of catalyst, the more HO• radicals. The last one will be considered as main oxidant species responsible for the photocatalytic process [46].

An increasing of photocatalyst quantity over the optimal limit leads to an augmentation of suspension turbidity, thus decreasing the intensity of UV radiation at its passing by the specimen, consequently resulting a decreasing of HO• radicals number generation.

The efficiency of Eosin Y discoloring increase with the increase in the concentration of photocatalysts (Fig. 8).

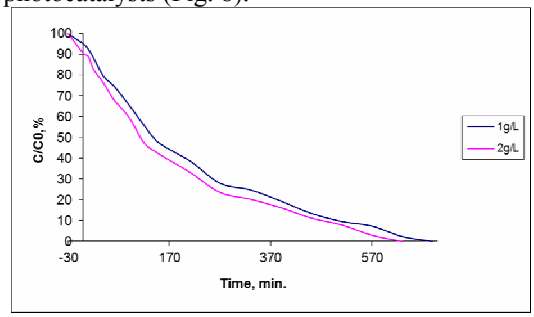

Fig. 8. *Efficiency of photocatalytic degradation of Eosin Y dye in the presence of Ag/SnO_2/clay nanocomposites catalysts samples*

4. Conclusions

We reported the synthesis and characterization of some new Ag/SnO_2/clay nanocomposites. Intercalation of argint/tin dioxide nanoparticles into clay was unambiguously proven by X-ray diffraction. The presence of nanoparticles in the samples was

verified by monitoring the specific surface area of the samples and the particle size distribution. It was established that this parameter increases because the crystallinity of nanocomposites increases. The ability of the nanocomposites to degrade Eosin Y dye under UV light was studied. It is observed that nanosized Ag/SnO_2/clay photocatalysts are an efficient photocatalyst, both in respect of decolorization as well as mineralization of Eosin Y. The synthesized Ag/SnO_2/clay nanocomposites are potential photocatalysts for treatment of organic wastewaters by converting the residual dyes to harmless compounds.

Acknowledgments

The financial support provided by the Research Contract within POSDRU No. /89/1.5/S/49944 Project, belonging to "Al.I.Cuza" University of Iasi.

References

[1]. Sikhwivhilu L.M., Pillai S.K., Hillie T.K. - *Influence of Citric Acid on SnO2 Nanoparticles Synthesized by Wet Chemical Processes*, Submitted to Journal of Nanoscience and Nanotechnology (Revised version).
[2]. Chappel S., Zaban A. - Sol. Energ. Mat. Sol. Cells. 71:141 (2002).
[3]. Schlamp M.C., Peng X., Alivisatos A.P. - J. Appl. Phys. 82:5837 (1997).
[4]. Cirera A., Vila A., Dieguez A., Cabot A., **Cornet A., Morante J.R.** - Sens. Actuat. B 64:65 (2000).
[5]. Miyauchi M., Nakajima A., Watanable T., Hashimoto K. - Chem. Mater. 14:2812 (2002).
[6]. Morales J., Perez V.C., Santos S., Tirado L.J., J. Electrochem. Soc. 143:284 (1996)
[7]. Aurbach D., Nimberger A., Markovsky B., Levi E., Sominski E., Gedanken A., Chem. Mater. 14:4155 (2002)
[8]. Artemyev M.V., Sperling V., Woggon U. - J. Appl. Phys. 81:6975 (1997)
[9]. Patent no. 2644284, 14/09/90 CLAL, *Nouveaux matériaux à base d'argent et d'oxide d'étain pour la réalisation de contacts électriques*.
[10]. Kameo A., Yoshimura T., Esumi K. - Colloids Surf. A: Physicochem. Eng. Aspects 215 (2003) 181–189.
[11]. Ullah M.H., Kim Il, Ha C.S. - Mater. Lett. 60 (2006) 1496–1501.
[12]. Zou X.Q., Ying E.B., Dong S.J., J. Colloid Interf. Sci. 306 (2007) 307–315.
[13]. Tian X.L., Wang W.H., Cao G.Y. - Mater. Lett. 61 (2007) 130–133.
[14]. Mohan Y.M., Lee K., Premkumar T., Geckeler K.E. - Polymer 48 (2007) 158–164.
[15]. Courrol L.C., Silva F.R., Gomes L. - Colloids Surf. A: Physicochem. Eng. Aspects 305 (2007) 54–57.
[16]. Chen Z.T., Gao L. - Mater. Res. Bull. 42 (2007) 1657–1661.
[17]. Khanna P.K., Singh N., Charan S., Viswanath A.K. - Mater. Chem. Phys. 92 (2005) 214–219.
[18]. Xu Guang-nian, Qiao Xue-liang, Qiu Xiao-lin, Chen Jian-guo - Colloids and Surfaces A: Physicochem. Eng. Aspects 320 (2008) 222–226.
[19]. Templeton A. C., Wuelfing W. P., Murray R. W. - Acc. Chem. Res. 33, 27 (2000).
[20]. Storhoff J. J., Mirkin C. A. - Chem. Re., 100, 409 (2000).
[21]. Shipway A. N., Katz E., Willner I. - Chem.Phys.Chem. (2000) 1, 18.
[22]. Zhong, C. J.; Maye - M. M. Ad . Mater. (2001) 13, 1507.
[23]. Kamat P. V. - Chem. Re. (1993), 93, 267.
[24]. Belloni J. - Radiat. Res. (1998), 150, 39.
[25]. Henglein A., Meisel D. J. - Phys. Chem. B (1998), 102, 8386.
[26]. Dimitrijevic N. M., Bartels D. M., Jonah C. D., Takahashi K., Rajh T. J. - Phys. Chem. B (2001), 105, 954.
[27]. Henglien A. Isr. - J. Chem. (1993), 33, 77.
[28]. Bruchez M., Moronne M., Gin P., Weiss S., Alivisatos, A. P. - Science (1998), 281, 2013.
[29]. Brust M., Bethell D., Keily C. J., Shiffrin D. J., Langmuir - (1998), 14, 5425.
[30]. Geirsig M., Pastoriza-Santos I., Liz-Marzan L. M. - J. Mater. Chem. (2004), 14, 607.
[31]. Link S., El-Sayed M. A. - J. Phys. Chem. B (1999) 103, 8410.
[32]. Musick M. D., Pena D. J., Botsko S. L., McEvoy T. M., Richardson T. N., Natan M. J. - Langmuir (1999), 15, 844.
[33]. Anjana Sarkar, Sudhir Kapoor, Tulsi Mukherjee - J. Phys. Chem. B (2005), 109, 7698 7704.
[34]. Popovici E., Hristodor C.M., Alexandroaei M., Hanu A.M. - Rev. Chem. 57: 8-11(2006).
[35]. Popovici E., Humelnicu D., Hristodor - C.M. Rev. Chem. (2006) 57: 675-678
[36]. Trillo J.M., Alba M.D., Castro M.A., Munoj A., Poyato J., Tobias M. - Clay Miner. 27, 423 (1992).
[37]. Miller S.E., Heath G.R., Gonzalez R.D. (1982) Clays ClayMiner. 30:111
[38]. Sowmiya M., Sharma A., Parsodkar S., Mishra B.G., Dubey A. (2007) Applied Catalysis A: General 333:272–280
[39]. Sposito G., Prost R., Gaultier J.P. - Clays Clay Miner. 31:9 (1983).
[40]. Rouquerol J., Rouquerol F., Sing K. - Adsorption by powders and porous solids, ISBN 10: 0-12-598920-2, Published: OCT-1998
[41]. Németh J., Dékány I., Süvegh K., Marek T., Klencsár Z., Vértes A., Fendler J. H. - Langmuir 19 (9):3762-3769 (2003).
[42]. Daneshvar N., Salari D., Khataee A.R., - J. Photochem. Photobiol. A: Chem. 157:111 (2003).
[43]. Kansal S.K., Singh M., Sud D. - Journal of Hazardous Materials 141:581–590 (2007).
[44]. Linsebigler A. L., Lu G. Q., Yates J. T. - *Photocatalysis on TiOn Surfaces: Principles, Mechanisms, and Selected Results*, Chem. Rev. 95 735–58, (1995).
[45]. Weiwei L., Guosheng L., Shuyan G., Shantao X., Jianji W. - Nanotechnology 19 (2008) 445711.
[46]. Nishio J., Tokumura M., Znad H.T., Kawase Y. - J. Hazard. Mater. B138:106-115 (2006).